Polar Mixtures under Nanoconfinement

Javier Rodriguez,[†,‡] M. Dolores Elola,[†] and Daniel Laria*[,†,§]

Departamento de Física, Comisión Nacional de Energía Atómica, Avenida Libertador 8250, 1429, Buenos Aires, Argentina, ECyT, UNSAM, Martín de Irigoyen 3100, 1650, San Martín, Provincia de Buenos Aires, Argentina, and Departamento de Química Inorgánica, Analítica y Química-Física e INQUIMAE, Facultad de Ciencias Exactas y Naturales, Universidad de Buenos Aires, Ciudad Universitaria, Pabellón II, 1428, Buenos Aires, Argentina

Received: June 24, 2009; Revised Manuscript Received: July 28, 2009

We present results from molecular dynamics simulations describing structural and dynamical characteristics of equimolar mixtures of water and acetonitrile, confined between two silica walls separated at interplate distances of $d = 0.6$, 1, and 1.5 nm. Two different environments were investigated: a first one where wall−solvent dispersion forces prevail (hydrophobic confinement) and a second one in which the terminal O atoms at the silica surface are transformed into silanol groups (hydrophilic confinement). For the former case, we found that, at the shortest interplate distance examined, the confined region is devoid of water molecules. At an interplate distance of the order of 1 nm, water moves into the confined region, although, in all cases, there is a clear enhancement of the local concentration of acetonitrile in detriment of that of water. Within hydrophilic environments, we found clear distinctions between a layer of bound water lying in close contact with the silica substrates and a minority of confined water that occupies the inner liquid slab. The bound aqueous layer is fully coordinated to the silanol groups and exhibits minimal hydrogen bonding with the second solvation layer, which exclusively includes acetonitrile molecules. Dynamical characteristics of the solvent mixture are analyzed in terms of diffusive and rotational motions in both environments. Compared to bulk mixtures, we found significant retardations in all dynamical modes, with those ascribed to water molecules bound to the hydrophilic plates being the most dramatic.

I. Introduction

Water−acetonitrile solutions represent prototype polar mixtures combining protic and aprotic components with important practical applications in many areas of chemistry such as chromatography,[1−3] electrochemistry,[4] and solvent extraction.[5] Under ambient conditions, the solvents fully mix at all compositions; however, as the temperature drops below $T \sim 270$ K, their solutions exhibit liquid−liquid phase coexistence.[6,7] At even lower temperatures, the phase diagram of the mixture presents a rich variety of heterogeneous equilibria, involving liquid and different solid phases as well.[8]

For quite a long time now, it has been well-known that confinement may modify the characteristics of phase equilibria of liquid mixtures.[9−11] For example, solvation within Vycor porous glasses affects the phase equilibria of water/lutidine[12] and the critical behavior of *n*-hexane/*n*-perfluorooctane[13] mixtures in a sensible fashion. Water−acetonitrile solutions are not exceptions: Recently, Kittaka et al.[14] reported calorimetric and infrared spectroscopy results that would suggest modifications in the bulk phase diagram of these mixtures, induced by the solvation in mesopores of the MCM-41 silicate,[15] with characteristic pore sizes intermediate between 2 and 4 nm.

In this paper, we will present molecular dynamics results of model systems mimicking water−acetonitrile mixtures confined between two parallel silica plates. Our work is mainly motivated by a series of recent computer simulation studies performed by Giovambattista et al.,[16−18] in which hydration under similar confinement conditions has been examined. By a series of careful modifications involving thermodynamic variables and the chemical surface composition of the confining plates, Giovambattista et al. found several solvation structures with well differentiated dynamical characteristics. In a much broader context, note that the study of liquid phases subjected to nanoconfinement is relevant not only from a fundamental, i.e., thermodynamic, perspective[19] but also for the correct interpretation of complex processes such as the folding of proteins,[20] chemical reactivity within reverse micelles,[21] nanofluidity,[22,23] and wetting and dewetting phenomena.[24,25]

Over the last 30 years, there has been a continuous interest in unraveling the molecular origins of the thermodynamic,[26−29] structural,[30−32] spectroscopic,[33−38] NMR,[3,39] and transport[40,41] properties of bulk water−acetonitrile solutions, along the whole composition range. At present, there seems to be a general consensus that the observed nonidealities exhibited by these solutions can be ascribed to concentration fluctuations, that would bring the solutions inhomogeneous at the mesoscopic scale. As such, the resulting structures of the mixtures would be the result of a complex interplay between packing effects and differences in the intramolecular connectivity (most notably those derived from the absence of hydrogen bonding in acetonitrile). Interestingly, these conclusions have also been predicted on theoretical grounds,[42,43] and validated by several computer simulation studies as well.[38,44,45]

Compared to the previous body of experimental and theoretical research, analyses of these mixtures in inhomogeneous environments are not that abundant: the list includes, in addition to the above-mentioned paper by Kittaka,[14] experimental[46,47] and theoretical[48,49] studies of liquid/vapor interfaces and mesoscopic

* Corresponding author. E-mail: dhlaria@cnea.gov.ar.
† Comisión Nacional de Energía Atómica.
‡ UNSAM.
§ Universidad de Buenos Aires.

10.1021/jp905920m CCC: $40.75
Published on Web 08/28/2009

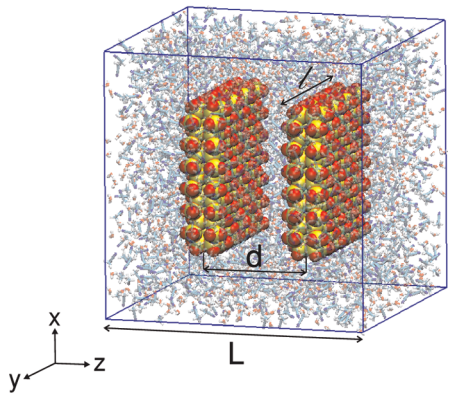

Figure 1. Geometrical arrangement of the simulation box.

binary clusters.[50] In what follows, we will present results for the solvation of equimolar mixtures of water−acentonitrile within confining environments, with characteristic size in the order of 1 nm. Two well differentiated scenarios were considered: in the first one, nonpolar plate−solvent interactions prevail (hydrophobic confinement), whereas, in the second, the external field acting on the mixture presents a more clear polar character (hydrophilic confinement). We will show that the presence of an aprotic cosolvent introduces new features in the resulting solvation structures, which differ at a qualitative level from what is found in the pure water cases. In one case, the changes involve total or partial water exclusion from the confined region, whereas, in the other, clear structural distinctions between interfacial and trapped water can be established. The latter inhomogeneities are also observed in the characteristics of the translation and rotational modes that dictate the dynamics of the solvents.

The organization of the present paper is as follows: In section II, we will describe details of the model and technical information about the simulation procedures. Section III includes results for equilibrium solvation structures of the mixtures, whereas, in section IV, we present results for time dependent properties. Concluding remarks are left for section V.

II. Model

The simulation experiments described in this paper correspond to systems containing a pair of silica plates, held at a fixed distance d, and immersed in an equimolar mixture of water (W) and acetonitrile (ACN). Initial configurations for these systems were generated from a trajectory of a bulk mixture comprising $N_W = N_{ACN} = 1860$ molecules, equilibrated at $p = 1$ bar and $T = 298$ K. Under these conditions, the simulation box length roughly fluctuated around $L \sim 60.5$ Å. After removing the necessary solvent to avoid plate−solvent overlaps (of the order of 200 molecules of each species), the pair of confining plates were inserted at positions $z = \pm d/2$, with their normal vectors aligned along the z -axis (see Figure 1). The resulting systems were then further equilibrated under ambient conditions, for an additional period of ∼2−3 ns, until the local concentrations of both solvents in the interplate region attained stable values.

For water−water interactions, we adopted the classical TIP3 model,[51] whereas interactions involving ACN molecules were taken from the Hamiltonian developed by Grabuleda et al.[52] The latter is a fully atomistic force field that includes intramolecular interactions described in terms of the stretching, bending, and dihedral contributions. The usual arithmetic and geometric combination rules were adopted to model W−ACN cross interactions. To establish a correspondence between our results and those reported in a series of previous simulations, experiments on hydration under confinement,[16−18,53] the model silica plates were identical to those described in ref 16. Briefly, each plate was modeled as a rectangular slab of thickness $\Delta = 8.66$ Å, exposing two square, (1.1.1) cristobalite faces of SiO_2, with side dimensions of $\ell = 31.15$ Å (see Figure 1).

In order to assess the importance of surface polarity on the resulting solvation structures and dynamics of the solvent mixture, terminal oxygen atoms lying at one of the two faces of each plate were transformed into charged O−H surface silanol groups. As such, two different restricted environments were examined: (i) a hydrophobic one (PHO−PHO), generated by approaching the nonfunctionalized interfaces, and (ii) a hydrophilic one (PHI−PHI), by approaching the polar hydroxylated interfaces.

Three plate-to-plate distances were considered: $d = 0.6$, 1, and 1.5 nm. The first two separations are comparable in size with the characteristic length scales describing interparticle spatial correlations in the bulk mixtures, while the last one is more comparable to the size of inhomogeneous mesoscopic W-rich and ACN-rich domains that have been invoked to rationalize experimental structural and dynamical characteristics of these mixtures.[43,45] Additional details pertaining to the geometrical atomic arrangement of the substrate and Hamiltonian parameters describing wall−solvent interactions can be found in ref 16.

Long range forces arising from Coulomb interactions were treated by implementing a particle-mesh Ewald sum procedure. Meaningful statistics were collected along 5 ns production runs. In all cases, we verified that solvent densities at large distances from the confined environment agree within ∼1% with the corresponding bulk values.[54]

III. Equilibrium Solvation Structures

A. PHO−PHO Arrangement. We will start our analysis by examining structural features of the confined mixed solvent, in the PHO−PHO arrangement. We will focus attention on site density fields along the z-direction of the type

$$g_\alpha(z) = \frac{1}{\rho_\alpha \ell}\left\langle \sum_i \delta(z_i^\alpha - z)\right\rangle \qquad (1)$$

where z_i^α is the z-coordinate of the ith site of species α, $\rho_\alpha = \langle \sum_i \delta(\mathbf{r}_i^\alpha - r)\rangle$ represents its average density in the bulk, and the angular brackets denote an equilibrium ensemble average. In the previous equation, the sum is restricted to those molecules whose coordinates satisfy $|x_i^\alpha| < \ell/2$ and $|y_i^\alpha| < \ell/2$.

In the top panels of Figures 2 and 3, we present results for spatial correlations associated to oxygen sites (α = W) and the central carbon atom (α = ACN), for the PHO−PHO arrangement, for the two limiting values of d investigated. Perhaps the most interesting observation that can be made from the direct inspection of both sets of results is the dramatic reduction of the water local concentration along the interplate region. Note that, for the shortest distance analyzed, $d = 6$ Å, the water $g_W(z)$ profile vanishes for $|z| < d/2$. On the other hand, the ACN profile looks like a wide peak, with a small indentation at the top, revealing that the structure of the confined solvent can be pictured in terms of a pair of layers, involving ∼20 molecules, in close contact with each one of the plates. At larger values of d, both solvents contribute to the interplate solvent populations, although still the ACN contribution is more prevalent. More precise quantitative estimates for the local ACN concentration

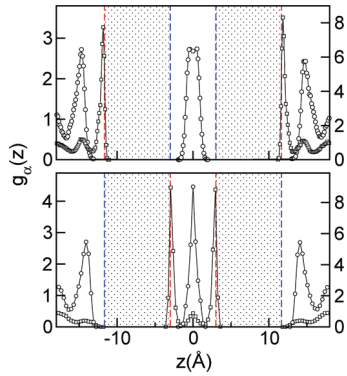

Figure 2. Density fields associated to W-oxygen (squares, right axis) and A-central-carbon sites (circles, left axis) for $d = 6$ Å. The results shown in the top (bottom) panel correspond to the PHO−PHO (PHI−PHI) arrangement. The shaded areas correspond to the volume excluded by the plates. Hydrophobic (hydrophilic) silica interfaces are rendered in blue (red).

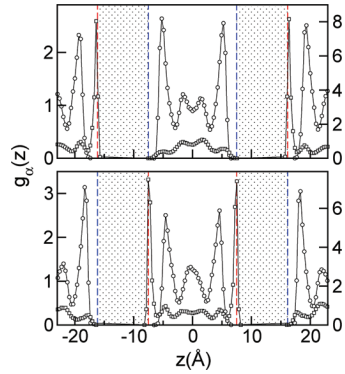

Figure 3. Same as Figure 1 for $d = 15$ Å.

TABLE 1: Solvation Parameters for Confined Water−Acetonitrile Mixtures

a. Hydrophobic Confinement

d (Å)	$e_{A/W}$	$\tilde{D}^{\parallel}_{W}$	$\tilde{D}^{\parallel}_{ACN}$	$\tilde{\tau}_{W}$	$\tilde{\tau}_{A}$
6	≳20		0.09 ± 0.03		8.7 ± 1.2
10	4.3	0.18 ± 0.06	0.17 ± 0.05	1.8 ± 0.4	5.7 ± 0.6
15	1.7	0.23 ± 0.06	0.20 ± 0.05	1.5 ± 0.3	3.1 ± 0.4

b. Hydrophilic Confinement

d (Å)	$e_{A/W}$ [a]	$\tilde{D}^{\parallel}_{W}$	$\tilde{D}^{\parallel}_{ACN}$	$\tilde{\tau}_{W}$	$\tilde{\tau}_{A}$
6	2.7[a]	∼0.03[b] ∼0.002[c]	∼0.01	∼17[c] ∼300[c]	∼50
10	2.5[a]	$0.13^{b} \pm 0.04$ ∼0.008[c]	0.07 ± 0.04	$5.8^{b} \pm 0.9$ ∼230[c]	8.1 ± 0.9
15	2.0[a]	$0.22^{b} \pm 0.05$ ∼0.01[c]	0.14 ± 0.08	$3.1^{b} \pm 0.4$ ∼130[c]	3.6 ± 0.7

[a] Only nonbound water was considered. [b] Confined nonbonded water. [c] Bonded water.

enhancement phenomenon can be obtained from the overall ratios of molar fractions

$$e_{A/W} = \frac{x_{ACN}}{x_{W}} = \frac{\bar{N}_{ACN}}{\bar{N}_{W}} \tag{2}$$

which are listed in the first column of Table 1a. In the previous equation, $\bar{N}_{\alpha} = N_{\alpha}(d/2)$, where $N_{\alpha}(z)$ denotes the cumulative integral,

$$N_{\alpha}(z) = \rho_{\alpha}/^{2} \int_{-z}^{z} g_{\alpha}(z')\, dz' \tag{3}$$

Note that, even at interplate distances as large as $d \sim 15$ Å, the value of $e_{A/W}$ is still of the order of ∼1.5.

These strong fluctuations in the local density fields for $d = 6$ Å are the results of combined effects arising from the confinement and the prevailing plate−solvent hydrophobic interactions. The comparison with the solvation at the external faces of the plates in the complementary PHI−PHI arrangement, where confinement effects can be safely discarded, is instructive (see the bottom panels of Figures 1 and 2). On the basis of the magnitudes of the main peaks of g_{A}, at the external interface, it is clear that plate−solvent hydrophobic interactions promote a local increment of the ACN concentration of similar magnitude than in the interplate region. However, the absence of confinement allows the appearance of a peak in $g_{W}(z)$ distribution, involving ∼10 water molecules, along the lateral 13 Å ≲ z ≲ 16 Å interval. Within this context, we also remark that the reduction of the water population in the confined region, which leads to the complete absence of water for $d \sim 5-6$ Å, is akin to the drying transition reported by Giovambattista et al.[16] for confined water in the same interplate distance range. This feature has been ascribed to a delicate interplay between the geometry of the environment and the thermodynamic properties of bulk and surface water, at the vicinity of its normal liquid−vapor phase equilibrium.

Orientational correlations provide supplementary information about the solvation under hydrophobic confinement. In Figure 4a, we present results for polarization densities of the type

$$\mu_{\alpha}(z) = \frac{1}{\rho_{\alpha}/^{2}} \left\langle \sum_{i} \delta(z_{i}^{\alpha} - z) \cos \theta_{i}^{\alpha} \right\rangle \tag{4}$$

where θ_{i}^{α} is the angle subtended between the z-axis and the dipole of the ith molecule of species α. At the shortest distances, $d = 6$ Å, the polarization along the z-axis presents two peaks of magnitude ∼ ±1, located at $z = \mp 0.75$ Å, which corresponds to the above-mentioned ACN molecules in close contact with the hydrophobic surfaces. Still, the magnitude of overall dipolar alignment along the z-direction is not relevant: a rough estimate of the average individual orientation of the molecules lying in close contact with the solid substrate can be inferred from the ratio of areas:

$$\overline{\cos \theta_{A}} \sim \frac{\int_{0}^{d/2} \mu_{A}(z)\, dz}{\int_{0}^{d/2} g_{A}(z)\, dz} \sim -0.05 \tag{5}$$

which shows that the ACN molecules remain practically with their dipole axis parallel to the plane of the hydrophobic interface. The sequence of slabs with positive and negative polarizations observed as we move from negative to positive values of z, which is also clearly perceptible in the positive z-axis in the profile for $d = 15$ Å (see top panel of Figure 4a), would indicate a layer-like ACN solvation structure, with antiparallel dipolar alignments. Concerning water orientations, the corresponding profiles in the confined region are featureless.

B. PHI−PHI Arrangement. The equilibrium solvation structures described in the previous section undergo sharp modifications under hydrophilic confinement. Results for solvent densities are shown in the two panels of Figure 3. In the

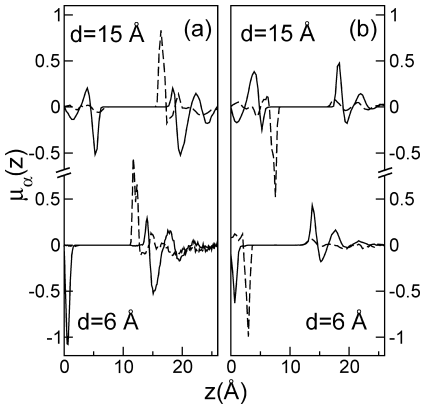

Figure 4. Orientational correlations for confined W−ACN mixtures at different interplate distances: (a) PHO−PHO arrangement; (b) PHI−PHI arrangement. The labeling is similar to that shown in Figure 1. Profiles for the negative portion of the z-axis are antisymmetric with respect to those shown in this figure.

interplate region, the profiles are clearly dominated by the O main peaks, located practically at $z = d/2$ (we recall that the spacing between the plates is given by the difference between the z-coordinates of the H atoms of the silanol groups). Moreover, the cumulative integrals reveal that these adsorbed layers, hereafter referred to as bound water (BW), include $N_{BW} \sim 40$ water molecules. Still, note that, in the central interplate region, one observes a clear enhancement of the acetonitrile concentration when it is compared to that of confined, albeit not bound, water (CNBW) molecules (a factor of ~ 2 for $d =$ 15 Å, see column 2 of Table 1b).

The position and the somewhat unusual magnitude of the BW peaks, $g_O(d/2) \sim 8$, indicate a large extent of structural stability worth investigating in more detail. The direct observation of a large series of configurations of the adsorbed W layers was useful to shed light on additional features. In particular, we observed that the adsorbed layers consist of regular, two-dimensional arrays of water molecules lying at interstices, equidistant from three adjacent silanol groups.[53] Concerning their intermolecular connectivity, these molecules exhibit clear double-donor−single-acceptor hydrogen-bond characteristics. The top panel of Figure 5 shows a snapshot of a typical configuration of a solvated hydroxylated silica substrate, in which this particular spatial arrangement and connectivity pattern are self-evident.

To validate this observation on more quantitative grounds, we computed the distribution function of OH intramolecular bond orientations for BW along the z-axis, namely,

$$P_{\cos\theta_{hb}}(\cos\theta) \propto \langle \sum_i \delta(\cos\theta_i^{OH} - \cos\theta)\rangle;$$
$$\cos\theta_i^{OH} = \frac{(\mathbf{r}_H^i - \mathbf{r}_O^i)\cdot\hat{\mathbf{z}}}{|\mathbf{r}_H^i - \mathbf{r}_O^i|} \quad (6)$$

Here, $\hat{\mathbf{z}}$ represents a unit vector, inward-pointing to each solid substrate, whereas the sum in eq 6 includes only BW molecules. The plot for the distribution corresponding to $d = 6$ Å is shown in the bottom panel of Figure 5. One observes a main peak at $\cos\theta \sim 0$, which is accordant with the W−silanol coordination described above, flanked by a much smaller lateral shoulder along $-1 \lesssim \cos\theta \lesssim -0.7$ that would indicate OH bonds pointing outward into the adjacent liquid phase. Interestingly, at this plate-to-plate separation range, this adjacent liquid phase

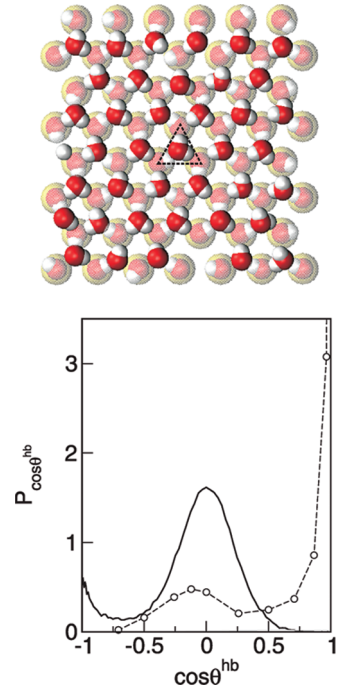

Figure 5. Top panel: Snapshot of a typical configuration of bound water (dark colors) adsorbed at the hydroxylated SiO_2 surface (light colors). The central triangle highlights the intermolecular connectivity of a bound water embedded between three silanol groups. Bottom panel: Distribution function for the projection of OH vectors along the z-axis for bound water molecules (solid line). The open circles correspond to results for trapped water taken from ref 53.

is practically devoid of W molecules and is composed exclusively by ~20 ACN molecules, with practically no participation of CNBW molecules. Consequently, the small number of out-of-plane OH bonds would act either as dangling groups or as potential hydrogen-bond donors to negatively charged N atoms in nearby ACN molecules.

At this point, it will be instructive to pause for a moment to establish similarities and differences between the previous description and the one reported by Lee and Rossky[53] for the hydration of a similar, albeit well separated, pair of hydrophilic surfaces. To facilitate the comparison, in Figure 5, we have included their results for $P_{\cos\theta^{hb}}$ reported in ref 53. For the latter case, note that a sizable number of OH groups of BW molecules point inward to the surface. As such, the "idealized" structures suggested by Lee and Rossky can be portrayed in terms of BW molecules coordinated to the silanol substrate from more external positions, with respect to the plane of the interface.

The overall picture of what emerges from this highly structured hydrophilic solvation pattern in mixtures suggests that it is the result of the combined effects arising from (i) the particular "architecture" of the hydroxylated cristobalite interfaces that provides an optimal arrangement of adsorption sites to easily accommodate solvents with sizes close to that of a water molecule; (ii) moreover, this geometrical arrangement leads to the saturation of the W−silanol intermolecular connectivity by means of a percolating network of in-plane hydrogen bonds; (iii) as a result, beyond this tightly bound water layer, the adjacent layer would be rich in ACN, revealing a drastic attenuation of the "hydrophilic character" of the original interface induced by the adsorbed aqueous layer; (iv) finally, packing effects arising from geometrical restrictions imposed by the confinement, combined with much weaker A−W interactions[55]—compared to W−silanol ones—would also contribute to "push" the BW layer deeper into the solid substrate.

Of course, these effects get somewhat milder as d increases: in the bottom panel of Figure 3, it is clear that the solvent layers adjacent to the BW also include a number of water molecules close to 10, a fact that would bring the overall scenario somewhat closer to the Lee−Rossky one (see also the profiles for the solvation of the external plate faces in the PHO−PHO arrangement). Before closing this section, we remark that the polarization profiles shown in the right panel of Figure 4 are accordant with the previous discussions: in the interplate region, water polarization along the z-axis remains even smaller than that for ACN which, in turn, maintains its oscillating character for the largest value of d considered.

IV. Dynamical Characteristics of Confined Mixtures

The solvation characteristics described in previous sections have interesting consequences on the dynamical side as well. Our analysis in what follows will be based on the examination of translational and orientational modes of each solvent. Following previous analyses, a rough estimate of the diffusive behavior of the confined solvents can be obtained from the temporal dependence of parallel displacements of the type

$$D_\alpha^{\parallel} = \lim_{t\to\infty} \frac{\mathscr{R}_\alpha{}^2(t)}{4t}$$

$$\mathscr{R}_\alpha{}^2(t) = \langle (x_\alpha^i(t) - x_\alpha^i(0))^2 + (y_\alpha^i(t) - y_\alpha^i(0))^2 \rangle \qquad (7)$$

where the correlation includes contributions from those molecules lying in the interplate region at times t and 0, exclusively. Results for $D_\alpha^{\parallel}$ for hydrophobic confinement are presented in the third and fourth columns of Table 1a. In order to single out confinement effects and minimize eventual deficiencies in the dynamical description provided by our choice for the Hamiltonian, the results are displayed in terms of $\tilde{D}_\alpha^{\parallel} = D_\alpha^{\parallel}/D_\alpha^{\mathrm{blk}}$, the fractional deviations with respect to bulk diffusion constants in the mixture. For the latter values, we obtained $D_{\mathrm{W}}^{\mathrm{blk}} = 2.95 \times 10^{-5}$ cm^2 s^{-1} and $D_{\mathrm{ACN}}^{\mathrm{blk}} = 2.90 \times 10^{-5}$ cm^2 s^{-1}, which are in reasonable agreement with the experimental results.[40]

The results for $\tilde{D}_\alpha^{\parallel}$ listed in Table 1a reveal drastic reductions in the diffusive dynamics of the mixtures, even for the longest distance considered. We remark that this overall slowdown of the translational modes is much more marked than the one reported for the pure water case, where the drop in the diffusive constant was found to be intermediate between 0.6 and 0.3, for similar values of d.[56] In fact, the direct comparison between the two sets of results, at the same value of d, is not totally adequate. Given the larger molecular size of ACN compared with W, we tend to believe that a more appropriate comparison could be established at similar values of $d^* = d/\bar{\sigma}$, where $\bar{\sigma}$ would be a length scale representative of an "average" molecular size of the mixture (without being too rigorous, say, $(\rho_{\mathrm{W}} + \rho_{\mathrm{A}})^{-1/3}$). We will not get deeper into this issue, since it is beyond the scope of the present article, although we remark that such a procedure would bring the two sets of results in much closer agreement.

Results related to the rotational dynamics of the mixtures are shown in the last two columns of Table 1a, where we display values of $\tilde{\tau}_\alpha$, the normalized time integrals of the single dipole autocorrelation function, namely,

$$\tilde{\tau}_\alpha = \frac{1}{\tau_\alpha^{\mathrm{blk}}} \int_0^\infty \frac{\langle \boldsymbol{\mu}_\alpha^i(t) \cdot \boldsymbol{\mu}_\alpha^i(0) \rangle}{\langle |\boldsymbol{\mu}_\alpha^i|^2 \rangle} \, \mathrm{d}t \qquad (8)$$

In the previous equation, $\boldsymbol{\mu}_\alpha^i$ represents the dipole of the ith confined molecule of species α. The entries in Table 1 were obtained from best fits, assuming a functional form for the dipole correlation function of the type $A_1 \exp(-t/\tau_1) + A_2 \exp(-(t/\tau_2)^\beta)$, and from the corresponding rotational relaxation time scales for the bulk mixtures: $\tau_{\mathrm{W}}^{\mathrm{blk}} = 7.7$ ps and $\tau_{\mathrm{ACN}}^{\mathrm{blk}} = 5.9$ ps. In addition to the somehow expected overall retardation, one observes that the hydrophobic confinement hinders the rotational motions of the trapped acetonitrile molecules in a much more sensible fashion than those for water. Moreover, the modifications in the rotational constants for the latter solvent are comparable to those observed for pure water under similar confinement conditions.[18]

Table 1b includes results for the dynamics under hydrophilic confinement. For these cases, we discriminated between BW and CNBW molecules. For the former case, note that translational and rotational characteristic time scales are between 1 and 2 orders of magnitude longer than in the previous cases. Moreover, in most cases, the magnitude of these temporal scales involves time spans of the order of several hundreds of picoseconds. Given the length of our simulations, our estimates are likely to be affected by a non-negligible degree of uncertainty due to the lack of statistics; as such, the values shown in Table 1b should be regarded only as qualitative indicators. Still, two observations are worth mentioning: (i) our results would confirm that, compared to the pure water solvation under similar conditions, the presence of a second, aprotic solvent provides an additional stability to the BW layer. In the $d \sim 1-1.6$ nm range, the increases in the corresponding $\tilde{\tau}$ are of the order of ~ 2,[18] while, here, the differences may go up to 2 orders of magnitude; (ii) contrasting with the pure water cases, no signs of nonmonotonic dynamical behavior—that would eventually manifest a decoupling between rotational and translational modes—was detected for these mixtures.[18]

V. Concluding Remarks

The results presented in this paper provide new insights concerning the behavior of polar mixtures, comprising protic−aprotic solvents, confined between two perfectly planar, silica surfaces. At sufficiently short interplate distances—$d \sim 0.6$ nm—water molecules get expelled from hydrophobic environments, a feature that resembles very much the drying transition observed under similar circumstances in aqueous solvation.[16] As d becomes of the order of ~ 1 nm, the entropic costs of such local concentration fluctuations are prohibitively high and water starts to get incorporated into the confined slab. Anyhow, even for interplate distances of the order of ~ 1.5 nm, the local water concentration within the confined region remains much smaller than that of acetonitrile. As a possible explanation to rationalize this feature, one could speculate that the resulting concentration fluctuations promote minimal disruptions in the water hydrogen bond connectivity imposed by the presence of the hydrophobic walls.[19] Anyhow, a more detailed analysis will necessarily include considerations pertaining to the characteristics of the fluctuations that take place in the neat solution at the mesoscale, an issue that has been examined in detail in several papers[43−45] and that will require further investigation.

Contrasting with the previous case, our results show that hydrophilic confinement does promote a net increment of water in the interplate region, although its local distribution is highly inhomogeneous. On the one hand, one observes a tightly bound water layer in close contact with the hydroxylated silica substrate. The unusual stability of this layer is made possible by the coincidence of an optimal geometrical arrangement of the surface that makes the embedding of water molecules in

specific sites possible, equidistant to three silanol groups. Moreover, the stabilization of this layer seems to be enhanced by the presence of a second solvation layer composed exclusively by acetonitrile that benefits BW−substrate interactions, in detriment of BW−solvent ones. This particular structure would be the result of the lack of out-of-plane OH groups available for coordination with more external water molecules. Beyond this second shell, and at sufficiently long interplate distances, one finds confined water−acetonitrile mixtures with local concentrations that resemble very much the hydrophobic scenario previously described.

The previous structural considerations have clear consequences on the dynamical side. In particular, the larger molecular size of the acetonitrile molecules enhances the overall retardation of the dynamical and rotational modes in hydrophobic environments, when the comparison is established with the pure water case, at similar values of *d*. These modifications are even more dramatic for the hydrophilic case, where diffusion and characteristic rotational times for BW and CNBW may differ up to 1 order of magnitude.

The applicability of the present results to a wider variety of polar mixtures, including protic−protic combinations, such as methanol−water, for example, is certainly an open question that deserves further investigations. The latter mixtures also present structural inhomogeneities in the mesoscopic range, although their characteristics differ from the ones encountered in W−ACN mixtures.[57] From a speculative perspective, we are led to believe that the similarities of the molecular dimensions of the two solvents and the additional possibility for methanol to act as a hydrogen bond donor, would render water−methanol scenarios somewhat closer to the ones for pure water. Investigations along these lines are currently being undertaken. However, we are confident that the physical implications derived from the results presented in this paper will remain enlightening for the correct interpretation of the behavior of polar mixtures within confining environments of more complex geometry and chemical characteristics than those presented here.

Acknowledgment. We are grateful to Prof. N. Giovambattista for providing the site coordinates of the confining plates. J.R., M.D.E., and D.L. are staff members of CONICET (Argentina).

References and Notes

(1) Parris, N. A. *Instrumental liquid chromatography*; Journal of Chromatography Library Series, Vol. 5; Elsevier: Amsterdam, The Netherlands, 1976.
(2) Braun, J.; Fouqueau, A.; Bemish, R. J.; Meuwly, M. *Phys. Chem. Chem. Phys.* **2008**, *10*, 4765.
(3) Dawson, E. D.; Wallen, S. L. *J. Am. Chem. Soc.* **2002**, *124*, 14210.
(4) See, for example: Couche, R. A.; Ritchie, I. M. *Aust. J. Chem.* **1984**, *37*, 231. Toma, H. E.; Takasugi, M. S. *J. Solution Chem.* **1989**, *18*, 575. Zhang, X. G.; Shi, Y. L.; Li, H. L. *J. Colloid Interface Sci.* **2002**, *246*, 296. Hoshi, N.; Haga, A.; Hori, Y. *Electrochemistry* **2004**, *72*, 852.
(5) See, for example: Schenck, F. J.; Wong, J. W. In *Analysis of Pesticides in Food and Environmental Samples*; Tadeo, J. L., Ed.; CRC Press: Boca Raton, FL, 2008; Chapter 6.
(6) Benter, G.; Schneider, H. *Ber. Bunsen-Ges. Phys. Chem.* **1973**, *77*, 997. Moolel, M.; Scheider, H. *Z. Phys. Chem. (Munich)* **1971**, *74*, 237. Szydłowski, J.; Szykyła, M. *Fluid Phase Equilib.* **1999**, *154*, 89.
(7) Sazonov, V. P.; Sha, D. G. *J. Phys. Chem. Ref. Data* 200*231*, 989.
(8) Scheinder, G. *Z. Phys. Chem.* **1964**, *41*, 327.
(9) Gelb, L. D.; Gubbins, K. E.; Radhakrishnan, R.; Sliwinska-Bartkowiak, M. *Rep. Prog. Phys.* **1999**, *62*, 1573. Gelb, L. D.; Gubbins, K. E. *Phys. Rev. E* **1997**, *55*, 1290. Gelb, L. D.; Sliwinska-BarkwowiakM.; Gubbins, K. In *Fundamentals of Adsorption*, 6th ed.; Maunier, F., Ed.; Elsevier: Paris, 1998; p 497.
(10) Rother, G.; Woywod, D.; Schoen, M.; Findenegg, G. H. *J. Chem. Phys.* **2004**, *120*, 11864. Woywod, D.; Schemel, S.; Rother, G.; Findenegg, G. H.; Schoen, M. *J. Chem. Phys.* **2005**, *122*, 125510.
(11) Greberg, H.; Patey, G. N. *J. Chem. Phys.* **2001**, *114*, 7182. Hemming, C. J.; Patey, G. N. *J. Phys. Chem. B* **2006**, *110*, 3764.
(12) Lin, M. Y.; Sinha, S. K.; Drake, J. M.; Wu, X. I.; Thiyagarajan, P.; Stanley, H. B. *Phys. Rev. Lett.* **1994**, *72*, 2207.
(13) Formisano, F.; Teixeira, J. *J. Phys.: Condens. Matter* **2000**, *12*, A351. Formisano, F.; Teixeira, J. *Eur. Phys. J. E* **2000**, *1*, 1.
(14) Kittaka, S.; Kuranishi, M.; Ishimaru, S.; Umahara, O. *Chem. Phys.* **2007**, *126*, 091103.
(15) Kresge, C. T.; Leonowicz, M. E.; Roth, W. J.; Vartuli, J. C.; Beck, J. S. *Nature* **1992**, *359*, 710.
(16) Giovambattista, N.; Rossky, P. J.; Debendetti, P. G. *Phys. Rev. E* **2006**, *73*, 041604.
(17) Giovambattista, N.; Debendetti, P. G.; Rossky, P. J. *J. Phys. Chem. C* **2007**, *111*, 1323.
(18) Romero-Vargas Castrillón, S.; Giovambattista, N.; Aksay, I. A.; Debendetti, P. G. *J. Phys. Chem. B* **2009**, *113*, 1438.
(19) Chandler, D. *Nature* **2007**, *455*, 831. Chandler, D. *Nature* **2005**, *437*, 640.
(20) See, for example: Rasaiah, J. C.; Garde, S.; Hummer, G. *Annu. Rev. Phys. Chem.* **2008**, *59*, 713.
(21) Levinger, N.; Swafford, L. *Annu. Rev. Phys. Chem.* **2009**, *80*, 395.
(22) Kolesnikov, A. I.; Zanotti, J.-M.; Loong, C.-K.; Thiyagarajan, P.; Moravsky, A. P.; Loutfy, R. O.; Burnhan, C. J. *Phys. Rev. Lett.* **2004**, *93*, 035503.
(23) Okazaki, M.; Toriyama, K. *J. Phys. Chem. B* **2003**, *107*, 7645.
(24) Poynor, A.; Hong, L.; Robinson, I. K.; Granick, S.; Zhang, Z.; Fenter, P. A. *Phys. Rev. Lett.* **2006**, *87*, 266101.
(25) Choudhyry, N.; Montgomery Pettitt, B. *J. Am. Chem. Soc.* **2007**, *129*, 4847.
(26) Morcom, K. W.; Smith, R. W. *J. Chem. Thermodyn.* **1969**, *1*, 503.
(27) Moreau, C.; Douhéret, G. *Thermochim. Acta* **1975**, *13*, 385.
(28) Moreau, C.; Douhéret, G. *J. Chem. Thermodyn.* **1976**, *8*, 403.
(29) Douhéret, G.; Moreau, C.; Viallard, A. *Fluid Phase Equilib.* **1985**, *22*, 289.
(30) Nishikawa, K.; Kasahara, Y.; Ichioka, T. *J. Phys. Chem. B* **2002**, *106*, 693.
(31) Takamuku, T.; Tabata, M.; Yamaguchi, A.; Nishimoto, J.; Kumamoto, M.; Wakita, H.; Yamaguch, T. *J. Phys. Chem. B* **1998**, *102*, 8880.
(32) I. Bakó, I.; Megyes, T.; Grósz, T.; Pálinkás, G.; Dore, J. *J. Mol. Liq.* **2006**, *125*, 174.
(33) Jamroz, D.; Stangret, J.; Lindgren, J. *J. Am. Chem. Soc.* **1993**, *115*, 6165.
(34) Tee, E. M.; Awichi, A.; Zhao, W. *J. Phys. Chem. A* **2002**, *106*, 6714.
(35) Bertie, J. E.; Lan, Z. *J. Phys. Chem. B* **1997**, *101*, 4111.
(36) Cringus, D.; Yeremenko, S.; Pshenichnikov, M. S.; Wiersma, D. A. *J. Phys. Chem. B* **2004**, *108*, 10376.
(37) Venables, D. S.; Schmuttenmaer, C. A. *J. Chem. Phys.* **1998**, *108*, 4935.
(38) Venables, D. S.; Schmuttenmaer, C. A. *J. Chem. Phys.* **2000**, *113*, 11222.
(39) Easteal, A. *Aust. J. Chem.* **1979**, *32*, 1379. Hardy, E. H.; Zygar, A.; Zeidler, M. D. *Z. Phys. Chem.* **2000**, *214*, 1633.
(40) von Goldammer, E.; Hertz, H. G. *J. Phys. Chem.* **1970**, *74*, 3734.
(41) Harris, K. R.; Newitt, P. J. *J. Phys. Chem. B* **1999**, *103*, 7015.
(42) Blandamer, M. J.; Blundell, N. J.; Burgess, J.; Cowles, H. J.; Horn, I. M. *J. Chem. Soc., Faradary Trans.* **1990**, *86*, 277.
(43) Marcus, Y.; Mignon, Y. *J. Phys. Chem.* **1991**, *95*, 400.
(44) H. Kovacs, J.; Laaksonen, A. *J. Am. Chem. Soc.* **1991**, *113*, 5596. Bergman, D. K.; Laaksonen, A. *Phys. Rev. E* **1998**, *58*, 4706.
(45) Mountain, R. D. *J. Phys. Chem.* **1999**, *103*, 10744.
(46) Zhang, D.; Gutow, J. H.; Eisenthal, K. B.; Heinz, T. F. *J. Chem. Phys.* **1993**, *98*, 5099.
(47) Kim, J.; Chou, K. C.; Somorjai, G. A. *J. Phys. Chem. B* **2003**, *107*, 1592.
(48) Paul, S.; Chandra, A. *J. Chem. Phys.* **2005**, *123*, 184706.
(49) Mountain, R. D. *J. Phys. Chem. B* **2001**, *105*, 6556.
(50) Molinero, V.; Laria, D.; Kapral, R. *J. Chem. Phys.* **1998**, *109*, 6844.
(51) Jorgensen, W. L.; Chandrasekhar, J.; Madura, J. D.; Impey, R. W.; Klein, M. L. *J. Chem. Phys.* **1983**, *79*, 926.
(52) Grabuleda, X.; Jaime, C.; Kollman, P. A. *J. Comput. Chem.* **2000**, *21*, 901.
(53) Lee, S. H.; Rossky, P. J. *J. Chem. Phys.* **1994**, *100*, 3334.
(54) Handa, Y. P.; Benson, G. C. *J. Solution Chem.* **1981**, *10*, 291. van Meurs, N.; Somsen, G. *J. Solution Chem.* **1993**, *22*, 427. Grande, M.; Alvarez-Juliá, J.; Barrero, C. R.; Marschoff, C. M.; Bianchi, H. L. *J. Chem. Thermodyn.* **2006**, *38*, 760.
(55) In equimolar mixtures, W−W coupling is stronger than that for A−W. See Table 1 in. Kovacs, H.; Laaksonen, A. *J. Am. Chem. Soc.* **1991**, *113*, 5596.
(56) See Figure 1 of ref 18.
(57) See, for example: Dixit, S.; Crain, J.; Poon, W. C. K.; Finney, J. L.; Soper, A. K. *Nature* **2002**, *416*, 829.

JP905920M